Estimation of deflections by interferometry in a cantilever array and its optimization based on a two-scale model

H. Hui[1], M. Lenczner[2*], S. Cogan[3], A. Meister[4], M. Favre[4], T. Overstolz[4], R. Couturier[5], S. Domas[5]

[1]FEMTO-ST, Time Frequency Department, University of Franche-Comté,
26, Chemin de l'Epitaphe, 25030 Besançon Cedex, France
[2]FEMTO-ST, Time Frequency Department, University of Technology at Belfort and Montbéliard,
26, Chemin de l'Epitaphe, 25030 Besançon Cedex, France
[3]FEMTO-ST, Applied Mechanics Department, CNRS, 26, Chemin de l'Epitaphe, 25030 Besançon Cedex, France
[4]CSEM , Rue Jaquet-Droz 1 CH-2002 Neuchâtel Switzerland
[5]University of Franche-Comte, LIFC, IUT Belfort-Montbéliard, Rue Engel Gros, 90000 Belfort, France
*Email: michel.lenczner@utbm.fr, Phone: +33 03 81 40 28 27

Abstract

In this paper, our attention is focused on a two-scale model based algorithm for deflection estimation of array of Atomic force microscopes (AFM) in quasi-static regime by interferometry. In a previous work, an algorithm based on three measurements by cantilever was introduced to compute their displacements in quasi-static regime. Here, we propose an improvement so that two measurements only are required. This is based on a published two-scale model of such array. Numerical simulation results of topographic scan by an array of AFMs on a sample surface are reported. The simulations are carried out with a model calibrated from a device which design optimization is also discussed here.

1. Introduction

Atomic force microscope (AFM) have been proven to be a very versatile tool for biotechnology and nanotechnology, since its invention in 1986 by Binnig et al. [1]. Cantilever displacement measurement plays a major role in AFM functioning. Various methods are possible, such as piezoresistivity, capacitive sensing and interferometry. Each of them has its own advantages and drawbacks. In this paper, we focus on a phase computation algorithm of interferometry measurement for arrays of AFMs. The paper [10] reports use of interferometry for parallel readout of a cantilever array. A technique extending the measurement range of interferometric cantilever arrays is presented in [4]. The simultaneous readout of multiple microcantilever arrays has been applied in various applications see [8].

In a previous work, we have reported an interferometry method for measuring displacement of cantilevers in quasi-static regime [6] where three measurements are necessary in each cantilever. A high speed camera is used to analyze the fringes. In view of real time applications, images are quickly processed and then a fast estimation method, based on a least square method, is used to determine the displacements of each cantilever. The algorithm achieves the wanted precision with fewer operations than a previous version based on a spline method [3]. However,

it is limited to arrays with uncoupled cantilevers. In this paper, we further improve the algorithm by reducing the number of measurements to two per cantilever. The method is based on a use of two-scale model which has been verified in [5]. A robust optimization design based on the same model are also reported.

2. Two-scale Model of Arrays of AFMs

The two-scale model governing elastic deflections in a one-dimensional array of AFMs, see Figure 4, introduced in [5], is restated in a way [7] appropriate to its implementation by the finite element method. The base and the cantilevers are modeled by the Euler-Bernoulli beam equation in the first component x_1 of the macroscopic variable and in the second component y_2 of the microscopic variable respectively.
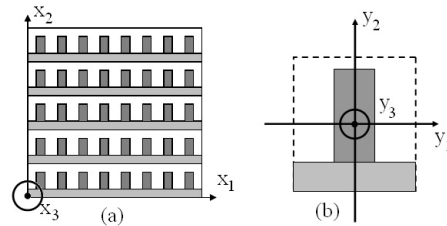

Figure 1. A one-dimensional view of (a) an Array and (b) a Cell.

The displacement can be decomposed on the orthogonal base of eigenmodes ψ_k,

$$u(t,.) = \sum_k U_k(t)\psi_k, \qquad (1)$$

with modal coefficients U_k. Each eigenmode is the product $\psi = \varphi^B \varphi^C$ of a base (or macroscopic) eigenmode $x_1 \mapsto \varphi^B(x_1)$ by a cantilever (or microscopic) eigenmode. The comparison of the model results to those of a direct finite element simulation shows a relatively good approximation of the eigenvalues associated to the transverse modes.

However, the comparison of solutions of the model in static or dynamic regime are not entirely satisfactory, see Figure 2 where computations are carried out with ten base modes φ^B and three cantilever modes φ^C which turns to be enough in this case. Same point forces of $20\mu N$ are applied at each probe tip in vertical direction.
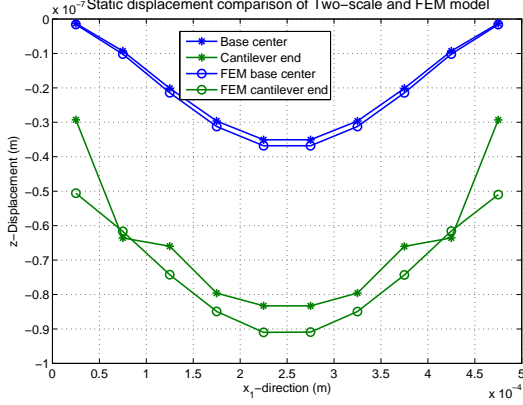

Figure 2. Static displacement comparison between direct FEM model and the two-scale model using the modal decomposition.

In addition, the approximation (1) is getting worse when the number of base modes increases. To circumvent this problem, in [6] we introduced the extension $\bar{u}$ of the displacement in the base as a function defined in cantilevers but independent of y_2. So, $\bar{u}$ is defined in the whole two-scale domain and we can define the difference $\widetilde{u} = u - \bar{u}$, also defined in the whole domain. In the base, it is obvious that $\widetilde{u} = 0$. We reformulate the motion equations for one-dimensional arrays of AFMs, satisfied by the couple $(\bar{u}, \widetilde{u})$,

$$
\begin{cases}
m^B \partial_{tt}^2 \bar{u} + R^B \partial_{x_1 \cdots x_1}^4 \bar{u} + \ell_C^0 R^C (\partial_{y_2 y_2 y_2}^3 \widetilde{u})_{|junction} \\
\quad = f^B \text{ in the base,} \\
m^C \partial_{tt}^2 \widetilde{u} + m^C \partial_{tt}^2 \bar{u} + R^C \partial_{y_2 \cdots y_2}^4 \widetilde{u} \\
\quad = F^C \text{ in cantilevers,}
\end{cases} \tag{2}
$$

where m^C, R^C and F^C are the linear mass density, the linear stiffness coefficient, and the load per unit length for cantilevers, and m^B, R^B, f^B and ℓ_C^0 are the effective linear mass, homogenized stiffness tensor, effective load per unit surface for base, and the cantilever width in the reference cell. In practice, we work on a model reduced at the microscopic scale through a modal decomposition on cantilever modes $\{\phi_k(y_2)\}_{k=1..n^C}$,

$$
\widetilde{u}(t, x_1, y_2) \approx \sum_{k=1}^{n^C} \widetilde{u}_k(t, x_1) \phi_k(y_2) \text{ and}
$$
$$
F^C(t, x_1, y_2) \approx \sum_{k=1}^{n^C} f_k^C(t, x_1) \phi_k(y_2).
$$

In this approximation, equations (2) yields,

$$
\begin{cases}
m^B \partial_{tt}^2 \bar{u} + R^B \partial_{x_1 \cdots x_1}^4 \bar{u} + \ell_C^0 R^C (\partial_{y_2 y_2 y_2}^3 \widetilde{u})_{|junction} \\
\quad = f^B \text{ in base,} \\
m^C \partial_{tt}^2 \widetilde{u}_k + m^C \partial_{tt}^2 \bar{u} \bar{\phi}_k + R^C \frac{\lambda_k^C}{(L_C^0)^4} \widetilde{u}_k \\
\quad = f_k^C \text{ for each } k,
\end{cases} \tag{3}
$$

where $\bar{\phi}_k = \int_0^{L_C^0} \phi_k \, dy_2$, $\phi_k(y_2) = \varphi_k(\frac{y_2}{L_C^0})$ and L_C^0 is the cantilever length in the reference cell. The eigenelements $(\lambda_k, \varphi_k)_{k \in \mathbb{N}}$ are solutions to the eigenvalue problem, posed in $(0, 1)$,

$$
\begin{cases}
\varphi_k'''' = \lambda_k^C \varphi_k & \text{in } (0, 1) \\
\varphi_k(0) = \varphi_k'(0) = 0, & \text{at } 0 \\
\begin{pmatrix} -\varphi_k''' \\ \varphi_k'' \end{pmatrix} = \lambda_k Q \begin{pmatrix} \varphi_k \\ \varphi_k' \end{pmatrix} & \text{at } 1.
\end{cases} \tag{4}
$$

where $Q = N \begin{pmatrix} J_0 & J_1 \\ J_1 & J_2 \end{pmatrix} N$ with $N = \begin{pmatrix} 1 & 0 \\ 0 & 1/L_C^0 \end{pmatrix}$ and $J_i = \int_{Y_R} (y_2 - L_C^0)^i \, dy$, $i = \{0, 1, 2\}$. The term Q is a contribution corresponding to the rigid AFM's tip. Then, $\bar{u}$ the displacement in base is solved using a classical finite element method coupled with a ordinary differential equation solver for the modal coefficients $\widetilde{u}_k$.

3. Measurement of Displacement in Arrays of AFMs

In this section, we detail our global phase computation algorithm of interferometry measurement for array of AFMs in quasi-static regime. Section 3-A describes the experimental set-up at CSEM, and Section 3-B presents the global phase computation algorithm.

A. The Experimental Set-up

An illustrative picture of the experimental set-up [3], developed by CSEM, is shown in Figure 3. In contrast to
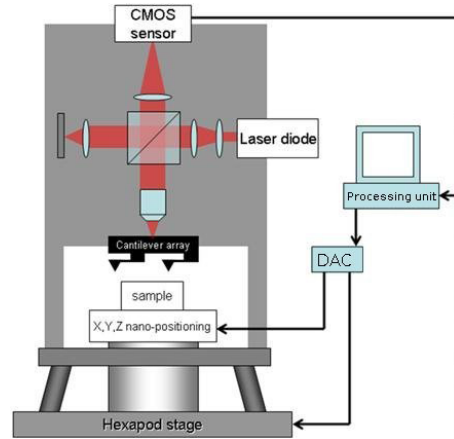

Figure 3. AFM experimental setup.

other optical based systems using a laser beam deflection scheme, which is sensitive to the angular displacement of the cantilever, interferometry is sensitive to the optical

path difference induced by the vertical displacement of the cantilever. The interferometric system is based on a Linnik interferometer [9]. A laser diode is first split into a reference beam and a sample beam that reaching the cantilever array. The complete system including a cantilever array and the optical system can be moved thanks to a translation and rotational hexapod stage with six degrees of freedom. Thus, the cantilever array is centered in the optical system which can be adjusted accurately. The beam illuminates the array by a microscope objective and the light reflects on the cantilevers. Likewise the reference beam reflects on a movable mirror. A CMOS camera chip records the reference and sample beams which are recombined in the beam splitter and the interferogram. Then, cantilever motion in the vertical direction produces lateral movements in the fringes of the interferogram. They are detected with the CMOS camera which images are analyzed by a LabView program to recover the cantilever deflections.

B. Cantilever Displacement Estimation

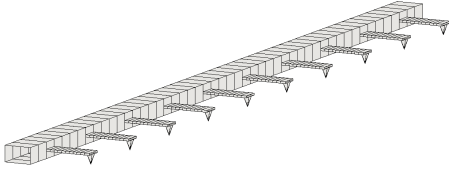We consider an array made with uncoupled rows of AFM cantilevers, see Figure 4.

Figure 4.   A one-dimensional view of array of AFMs.

In [3], as shown in Figure 5, the cantilever is covered by interferometric fringes. They distort when cantilevers are deflected. For each cantilever, the displacement is derived from phase shift of the light intensity. A phase shift corresponds to the lateral shift of the intensity profile along a segment of pixels induced by the cantilever bending. Three segments of pixels, parallel to its width, are used. The first one is located just above the AFM tip (tip profile), it provides the phase shift modulo 2π. The second one is close to the base junction (base profile) and is used to determine the exact multiple of 2π through an operation called unwrapping where it is assumed that the displacements along the two measurement segments are linearly dependent. The third one is on the base (reference profile) and provides a reference for cancelling the effect of base motion.

Each profile is expressed in a normalized interval $(0, M-1)$ where M is the number of pixels of the profile. The gray-level light intensity is under the form $a\xi + b + A\cos(2\pi f\xi + \theta)$ where $\xi \in (0, M-1)$, f and θ are the frequency and the phase of the interferometric signal, and the affine function $a\xi + b$ corresponds to cantilever surface tilt with respect to the light source. The linear
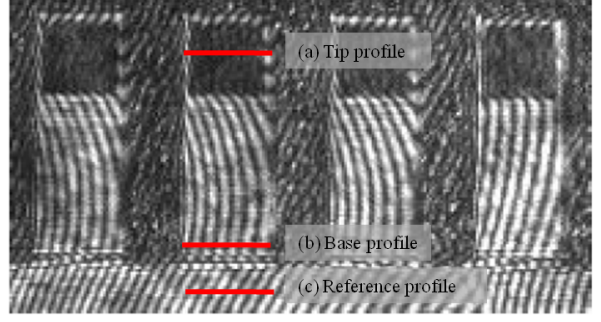

Figure 5.   Intensity profiles in cantilevers: (a) above the tip; (b) close to base-cantilever junction.

term $a\xi + b$ is estimated thanks to a linear least-square method. So, in the following, we consider only the cosine part,

$$I(\xi) = A\cos(2\pi f\xi + \theta). \qquad (5)$$

The phase computation is done either using a spline method or a least square method detailed in [2]. For a given phase θ, we denote by $\theta^* \in [0, 2\pi)$ its value modulo 2π i.e.

$$\theta = \theta^* + 2n\pi \text{ and } n = \left[\frac{\theta}{2\pi}\right], \qquad (6)$$

where $[\alpha]$ represents the integer part of α. The relation between the phase and the displacement is $\theta = 2\pi f\bar{c}(\bar{b} - 2u)$ where $\bar{b}$, $\bar{c}$ are constants related to the tilt of the beam splitter and are determined in a calibration phase. Moreover, the constant $\bar{b}$ corresponds to a constant phase shift that is ignored in the following, so we use only the proportionality relation

$$\theta = -mu. \qquad (7)$$

As u is decomposed into $\bar{u} + \tilde{u}$, the phase θ is also decomposed as $\theta = \bar{\theta} + \tilde{\theta}$. The base and tip profiles are taken at positions $y_2 = y_{2,1}$ and $y_{2,2}$ and all corresponding notations are indexed by 1 and 2, as for instance θ_1 and θ_2. In the setup [3], the reference profile is used to determine $\bar{\theta}$. The displacements of the base are assumed to be sufficiently small so that $\bar{\theta}^* = \bar{\theta}$. The base profile is sufficiently close from the base so that $\theta_1 = \theta_1^*$ also. And, the linear relation between $\tilde{u}_1$ and $\tilde{u}_2$, or $\tilde{\theta}_1$ and $\tilde{\theta}_2$, is used to determine the integer n_2. In total, $\bar{u}$, $\tilde{u}_1$ and $\tilde{u}_2$ are determine from three measurements and the tip force can be deduced.

In the following, we introduce an alternate method to avoid the reference measurement, based on the two-scale model.

For an array of N cantilevers, we refer the ith cantilever with the subscript $i \in \{1, ..., N\}$, and we use the relation (7) applied to each of them,

$$\begin{cases} \theta_{1,i} = \theta_{1,i}^* = -m(\bar{u}_i + \tilde{u}_{1,i}), \\ \theta_{2,i} = -m(\bar{u}_i + \tilde{u}_{2,i}). \end{cases}$$

The above equation written in vector form is

$$\begin{cases} \Theta_1 = \Theta_1^* = -m(\bar{U} + \tilde{U}_1), \\ \Theta_2 = -m(\bar{U} + \tilde{U}_2). \end{cases} \quad (8)$$

The two-scale model is discretized, and the N-dimensional vectors $\bar{U}$, $\tilde{U}_1$ and $\tilde{U}_2$ represent the displacements in the base and in cantilevers at $y_2 = y_{2,1}$ and $y_{2,2}$ respectively at the coordinates x_1 of the cantilever centers. Neglecting all external forces excepted the tip forces $f^{tip} = (f_i^{tip})_{i=1,...,N}$ and considering the system in the quasi-static regime, there exists three $N \times N$ stiffness matrices $\bar{K}$, $\tilde{K}_1$ and $\tilde{K}_2$ such that

$$\bar{U} = [\bar{K}]^{-1} f^{tip}, \ \tilde{K}_1 \tilde{U}_1 = f^{tip} \text{ and } \tilde{K}_2 \tilde{U}_2 = f^{tip}. \quad (9)$$

Eliminating f^{tip} in the two last relations using the first one,

$$\begin{cases} \bar{U} = [\bar{K}]^{-1} \tilde{K}_1 \tilde{U}_1, \\ \tilde{U}_2 = [\tilde{K}_2]^{-1} \tilde{K}_1 \tilde{U}_1. \end{cases} \quad (10)$$

By (8) and (10), we derive the relation between the phases of two profile lines,

$$\Theta_2 = K\Theta_1 \quad (11)$$

where the matrix $K = ([\bar{K}]^{-1} + [\tilde{K}_2]^{-1}) \tilde{K}_1 ([\bar{K}]^{-1} \tilde{K}_1 + Id)^{-1}$ and Id being the identity matrix. Using this relation and the fact that $\Theta_1 = \Theta_1^*$ we deduce n_2 in the phase decomposition (6) and Θ_2,

$$n_2 = \left[\frac{K\Theta_1^*}{2\pi} \right] \text{ and } \Theta_2 = \Theta_2^* + 2n_2\pi. \quad (12)$$

Thus, combining the relations (8), (9) and (12) we can establish that

$$\Theta_1^* = D_1 f^{tip} \text{ or } \Theta_2^* + 2n_2\pi = D_2 f^{tip}$$

with $D_1 = -m([\bar{K}]^{-1} + [\tilde{K}_1]^{-1})$ and $D_2 = -m([\bar{K}]^{-1} + [\tilde{K}_2]^{-1})$. In conclusion, we estimate the tip forces from (9) and we deduce $\bar{U}$ the base displacement and U_2 the total tip displacement, all being expressed with the measurements Θ_1^* and Θ_2^*,

$$f^{tip} = D_1^{-1} \Theta_1^* \text{ or } f^{tip} = D_2^{-1}(\Theta_2^* + 2n_2\pi), \quad (13)$$

$$\bar{U} = [\bar{K}]^{-1} f^{tip}, \ U_2 = -\frac{1}{m}(\Theta_2^* + 2n_2\pi) \text{ with (12)}. \quad (14)$$

In practice, the formula (12) may produce inaccurate phase of tip profile by a perturbation of 2π. The source of the error comes from the integer part calculation due to its discontinuity. We state Algorithm 1 that eliminates the error, where ε is in the range of the error.

Algorithm 1: Phase correction algorithm.

1   $\Theta_1 \leftarrow$ phase of the base profile
2   $\Theta_2 \leftarrow$ First tip-profile phase estimated by (12)
3   $\Theta_2' \leftarrow$ Second tip-profile phase estimated by (11)
4   $\delta\Theta_2 = \Theta_2' - \Theta_2$
5   $\Theta_2 = \Theta_2 + 2\pi * round(\frac{\Theta_2}{2\pi})$

---

4. Robust Design Optimization for Arrays of AFMs

Parameters of an array, such as the cantilever length, width and thickness, spring constant and deflection angle of the cantilevers for a given force, footprint of the array and lateral pitch between two adjacent cantilever, must satisfy initial requirements for good operation. Thanks to SIMBAD a decision making tool for development design, which we introduced in [6], we perform various optimization analyzes for the design of AFM probe arrays. The applications of this robust optimization tool are shown for one-dimensional arrays of AFM design. Two dimensional arrays with unconnected rows are made by aligning several one-dimensional arrays. We consider designing six types of array of AFMs on a single wafer. The 6 types of arrays correspond to 3 different cantilever spring constants, and to two different cantilever pitch conditions. For some applications, the pitch between cantilevers cannot be freely chosen. The three spring constants correspond to 0.03, 0.3 and 3 N/m, and the two pitch conditions define the lateral and longitudinal cantilever pitches as a multiple of 10, respectively 100 μm. After definition of the boundary conditions, such as minimal and maximal values of the parameters to be optimized and material properties, SIMBAD computes the optimal design of the probe arrays.

Table 1 summarizes the results of the optimization computation. A microfabrication run to produce cantilever
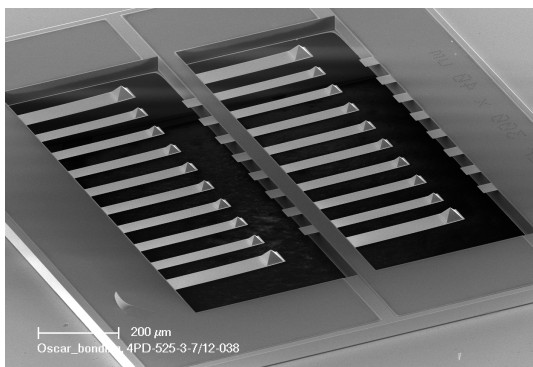
Table 1. Designs of probe arrays defined using the design decision making tool SIMBAD. The values in italic correspond to the initial conditions, and the values in bold to the optimized design parameters.

Array design	1	2	3	4	5	6
Pitch condition [μm]	*10*	*10*	*10*	*100*	*100*	*100*
Spring constant [N/m]	*0.03*	*0.3*	*3*	*0.03*	*0.3*	*3*
No. lever in x-direction	**16**	**16**	**11**	**10**	**10**	**10**
No. lever in y-direction	*2*	*4*	*5*	*2*	*3*	*5*
Pitch in x-direction [μm]	**60**	**60**	**90**	**100**	**100**	**100**
Pitch in y-direction [μm]	**500**	**250**	**200**	**500**	**300**	**200**
Length of cantilever [μm]	**300**	**150**	**100**	**300**	**150**	**100**
With of cantilever [μm]	**40**	**40**	**56**	**40**	**40**	**56**
Optimized spring constant	**0.033**	**0.33**	**2.7**	**0.033**	**0.33**	**2.7**

arrays with the optimized design was launched. An example of a computed optimized design and of a produced cantilever array are shown in Figure 6.

5. Numerical Simulations

We illustrate the algorithm by a sample surface topographic scan simulation for an array of AFMs in quasi-static regime. We consider an 10-cantilevers array with base dimensions $L_B \times \ell_B \times h_B = 500\mu m \times 16.7\mu m \times 10\mu m$, and those of cantilevers $L_C \times \ell_C \times h_C = 25\mu m \times 10\mu m \times 1.25\mu m$. The other model parameters are the bending coefficient $R^B = 1.09 \times 10^{-5} N/m$, $R^C = 2.13 \times 10^{-4} N/m$ and the masses per unit length $m^B = 0.0233kg/m$, $m^C = 0.00291kg/m$, and the light wavelength is $\lambda = 0.633\mu m$. The number of pixels in all measurement segments is taken as 20. The position of the base profile line is defined

Figure 6. Example of an optimized design geometry. The larger cantilevers with larger and higher tip situated in the corner of the probe array are used to land and adjust the probe array onto the sample surface.

as $y_{2,1} = \frac{L_C^0}{10}$. The topography of the samples is defined with bumps that are regularly distributed both in x_1- and y_2-directions, see Figure 7.
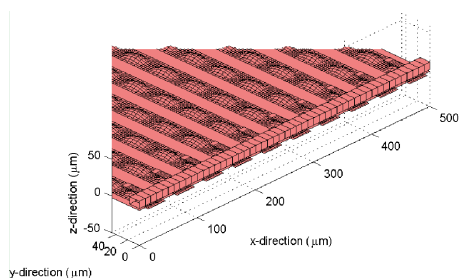

Figure 7. AFM arrays and samples.

The scan procedure is following:

1) The AFM arrays is a low position to put tips in contact with the sample surface.
2) The scanner moves in the negative y_2-direction and the deflection at tips are measured by interferometry in each scan step.
3) At the end of the line, the scanner moves back to the initial y_2-position, then increase the x_1-position to the next line.
4) Repeat step 2 and 3 until the required number of lines is obtained.
5) Save data.

All these steps together with the method for estimation of cantilever deflection have been implemented in a simulation. The sample is an array of 10×10 bumps. Their dimensions are $L_S \times \ell_S \times h_S = 10\mu m \times 20\mu m \times 0.1\mu m$. Twenty scan lines distant from $2\mu m$ are recorded in the x_1-direction with 128 scan points each distant from $1\mu m$. The estimated three-dimensional topography with Formula (12) is presented in Figure 8.

It shows peaks due to the integer part calculation in Formula (12). The use of Algorithm (1) eliminates them
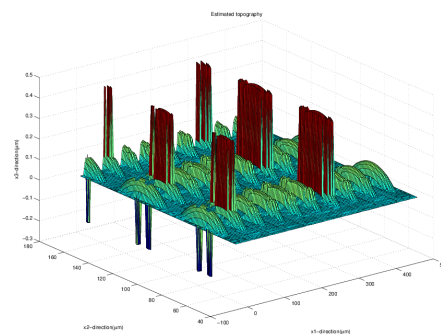

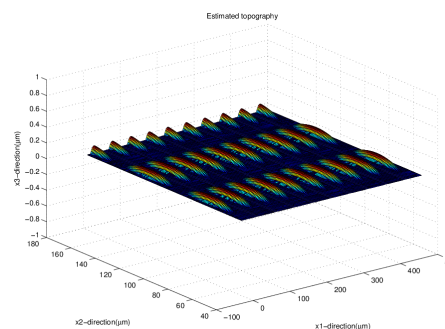Figure 8. Estimated sample topography with Formula (12).

as seen in Figure 9.

Figure 9. Estimated sample topography after phase correction.

6. Conclusion

In this paper, we have presented an effective global phase computation algorithm of interferometry for deflection measurement in an array of cantilevers in quasi-static regime. It improves a method using three measurements in each cantilever by avoiding one of them. It has been tested in a full simulation including a cantilever array, a scanner and an analyzed surface. We have also reported results of design optimization for an array of AFMs. It opens the way for future works on model calibration, other design problems, such as for dynamical problem, and for control synthesis. Applications are also envisionned as for instance topographic scans for different samples and force spectroscopy.

7. Acknowledgements

References

[1] G. Binnig, C.F. Quate, and C. Gerber. Atomic force microscope. *Physical Review Letters*, 56(9):930 – 3, 1986.

[2] R. Couturier, S. Domas, G. Goavec-Merou, M. Favre, M. Lenczner, and A. Meister. A new approach based on a least square method for real-time estimation of cantilever array deflections with an fpga. *Design, Control and Software Implementation for Distributed MEMS (dMEMS), 2012 Second Workshop on*, pages 30–37, 2-3 April 2012.

[3] M. Favre, J. Polesel-Maris, T. Overstolz, P. Niedermann, S. Dasen, G. Gruener, R. Ischer, P. Vettiger, M. Liley, H. Heinzelmann, and A. Meister. Parallel afm imaging and force spectroscopy using two-dimensional probe arrays for applications in cell biology. *Journal of Molecular Recognition*, 24(3):446–452, 2011.

[4] Sanchitha Fernando and Michael W. Austin. Extending the deflection measurement range of interferometric microcantilever arrays. *Journal of microelectromechanical systems*, 18(2):480–487, 2009.

[5] H. Hui, M. Lenczner, E. Pillet, and S. Cogan. A two-scale model for one-dimensional arrays of cantilevers and its verification. *Mechatronics*, 22(5):538 – 543, 2012.

[6] H. Hui, Y. Yakoubi, M. Lenczner, S. Cogan, A. Meister, M. Favre, R. Couturier, and S. Domas. Modeling, filtering and optimization for afm array. *Thermal, Mechanical and Multi-Physics Simulation and Experiments in Microelectronics and Microsystems (EuroSimE), 2011 12th International Conference on*, pages 1/6 – 6/6, 18-20 April 2011.

[7] Hui Hui, Youssef Yakoubi, Michel Lenczner, Nicolas Ratier, et al. Semi-decentralized approximation of a lqr-based controller for a one-dimensional cantilever array. In *Proceedings of the 18th IFAC World Congress, 2011*, volume 18, pages 1422–1428, 2011.

[8] Sven Kelling, François Paoloni, Juzheng Huang, Victor P. Ostanin, and Stephen R. Elliott. Simultaneous readout of multiple micro-cantilever arrays with phase-shifting interferometric microscopy. *Review of Scientific Instruments*, 80(9):093101, 2009.

[9] M. B. Sinclair, M. P. de Boer, and A. D. Corwin. Long-working-distance incoherent-light interference microscope. *Applied Optics*, 44(36):7714–7721, 2005.

[10] T. Sulchek, R.J. Grow, G.G. Yaralioglu, S.C. Minne, C.F. Quate, S. R. Manalis, A. Kiraz, A. Aydine, and A. Atalar. Parallel atomic force microscopy with optical interferometric detection. *Applied Physics Letters*, 78(12):1787–1789, 2001.